Hindawi
Geofluids
Volume 2022, Article ID 9430526, 11 pages
https://doi.org/10.1155/2022/9430526

Research Article

A Prediction Method for Floor Water Inrush Based on Chaotic Fruit Fly Optimization Algorithm–Generalized Regression Neural Network

Zhijie Zhu,[1,2] **Chen Sun**,[1] **Xicai Gao**,[2] **and Zhuang Liang**[3]

[1]*School of Mining, Liaoning Technical University, Fuxin, China*
[2]*State Key Laboratory of Coal Resources in Western China, Xi'an University of Science and Technology, Xi'an, China*
[3]*Research Centre, Ministry of Emergency Management, China*

Correspondence should be addressed to Zhijie Zhu; zhuzhijie@lntu.edu.cn

Received 30 March 2022; Revised 10 May 2022; Accepted 8 June 2022; Published 20 June 2022

Academic Editor: Zhijie Wen

The research was aimed at predicting floor water-inrush risk in coal mines and forewarn of such accidents to guide safe production of coal mines in practice. To this end, a prediction method for floor water inrush combining the chaotic fruit fly optimization algorithm (CFOA) and the generalized regression neural network (GRNN) is proposed. Floor water inrush is predicted by virtue of the robust nonlinear mapping capability of the GRNN. However, because the prediction effect of the GRNN is influenced by the smoothing factor, the CFOA is adopted to optimize this factor. In this way, influences of human factors during parameter determination of the GRNN prediction model are decreased, and the prediction accuracy and applicability of the model are improved. Results show that the CFOA–GRNN prediction model has an accuracy of 93.2% for whether floor water inrush will occur or not. Compared with the BPNN, RNN, and GRU network prediction model, the CFOA–GRNN model is superior in the prediction accuracy and generalization, and it can more accurately predict floor water inrush.

1. Introduction

With the increasing depletion of shallow coal resources and the increasing intensity of coal mining, more and more coal mines will encounter deep mining issues [1–5]. Compared with shallow coal mining, deep rock mass is in a typical complex mechanical environment of "three highs and one disturbance" (high ground stress, high karst water pressure, high ground temperature, and strong mining disturbance), showing large deformation and uncoordinated deformation and impact deformation [6–15]. Due to the characteristics of deep rock mechanics that are significantly different from those of shallow rock mechanics, coupled with the complexity of the occurrence environment, a series of catastrophic accidents in deep resource mining have greatly increased in frequency, intensity, and scale. Coal-rock dynamic disasters such as pressure appearance, floor water inrush, mine earthquake, rock burst, and coal and gas outburst become more frequent, and the disaster mechanism will become more complex [16]. In recent years, several major accidents in coal mines in my country are mostly secondary disasters, which have caused the expansion of accidents and increased the catastrophic nature of accidents. For example, in 2005, Fuxin Sunjiawan Coal Mine caused coal and gas outbursts due to rock bursts, and then, a huge gas explosion occurred, killing 214 people and injuring 30 people. During the mining of the 4th coal seam in Huafeng Coal Mine, due to the frequent occurrence of rock bursts, a large amount of water from the roof abscission flowed into the working face. As mining depths increase, coal seams bear increasing karst aquifer pressure, and therefore, the floor water-inrush risk increases: this has been one of the greatest hidden dangers for safe production of coal mines in China. In such context, predicting floor water-inrush risk is important in preventing accidents arising from such disasters in coal mines and ensuring safe mining above high-pressure aquifers.

Much theoretical analysis and numerical simulation has been conducted on the principle and prediction of water inrush from coal floors. For examples, Hu et al. [17] built a physical model with similar materials of the fracture zone in the synclinal axis above a confined aquifer and studied the mechanism of floor water inrush under the combined effect of a confined aquifer and a fracture zone. Numerous scholars also evaluated the influences of confining pressure and permeation pressure on water inrush from coal floors and obtained the mechanism of water inrush from coal floors under the coupled effect of seepage field and stress field [18–21], studied the effects of faults on stability of the aquifuge of coal floors, deduced the critical water pressure formula for failure of the aquifuge under influences of the fault, and proposed the corresponding mechanical criterion for floor water inrush. Li and Wang [22] reproduced the formation and evolution process of water-inrush channels through numerical simulation using FLAC (3D), which provides insights into formation and evolution characteristics of water-inrush channels in coal floors under high pressure. Ma et al. [23] combined theoretical analysis and numerical simulation with rock failure process analysis and microseismic monitoring to study failure characteristics and damage depth of coal floors above a confined aquifer. The method overcomes the limitations of a single method in previous research and also provides a reference for solving the water-inrush problems in roadways and selection of proper reinforcement measures. Shao et al. [24] proposed a catastrophe prediction model for floor water inrush in coal mines and deduced formulae for critical stress and energy release at failure of the floor system, providing a new theoretical approach for predicting water inrush from coal floors. By using the Mohr–Coulomb criterion and theory of fracture mechanics, Zhang et al. [25] studied the failure mechanism of floor water inrush and found that the higher the breaking energy of fractures, the more significant the floor water-inrush risk in coal mines. Existing theoretical formulae for floor water inrush generally only consider a few influencing factors and therefore are inapplicable to other coal mines. In addition, laboratory tests simplify the mining conditions, so the results are only of reference significance in prediction. Although numerical calculation method develops apace, it is still unable to simulate the complex geological and hydrogeological conditions encountered in deep mining.

In recent years, several risk evaluation methods and prediction models from multiple aspects have been proposed based on nonlinear statistical theory. Zhang and Yang [26] proposed a dynamic GRU (gated recurrent unit) neural network prediction model, the model is able to predict water inrush from coal floor with high accuracy. Zhang et al. [27] established a MFIM-TOPSIS variable weight model, which combines a multifactor interaction matrix (MFIM) and the technique for order performance by similarity to ideal solution (TOPSIS) to implement the risk assessment of floor water inrush in coal mines. Zhang et al. [28] presented a mathematical assessment method for coal-floor water-inrush risk integrating the hierarchy-variable-weight model (HVWM) with collaboration-competition theory (CCT). Zhao et al. [29] proposed a novel and promising assessment model for water inrush based on random forest (RF), which was more practicable to assess the water-inrush risk than PNN. Dong et al. [30] combined the Fisher feature extraction and support vector machine (SVM) methods, and this new combined model was more accurate and efficient in discriminating water-inrush sources than the traditional SVM model. Wang et al. [31] established PCA- (principal component analysis-) BP (Back Propagation) neural network classification model which can effectively identify coal mine water inrush. These methods have been applied in practical work, while still showing certain drawbacks. For instance, the distance discriminant analysis correlates the discriminant distance with units of indices and considers various different indices and variables equally, which sometimes fails to meet the actual requirements, thus leading to less accurate predictions. The SVM does not provide general solutions to nonlinear problems, so it needs to be further improved. The BP neural networks have shortcomings that the BP neural network needs a large number of data samples for training and also has too many optimized parameters [32].The generalized regression neural network (GRNN) is a kind of radial basis function neural network proposed by Specht, which has a strong ability for nonlinear mapping [33]. Compared with the BPNN and the SVM, the GRNN has fewer adjustment parameters, does not easily fall into local minima, and is good at processing large-scale training samples. The generalized regression neural network (GRNN) is highly superior in approximation capability, learning rate, and prediction accuracy, and it can reduce computation complexity and better predict floor water-inrush risk [34, 35].

On this basis, the GRNN model is established to predict floor water inrush based on the theory of nonlinear regression by combining relevant water-inrush data of numerous working faces. At the same time, the chaotic fruit fly optimization algorithm (CFOA) is used to optimize the smoothing factor of the GRNN. The novelty of CFOA-GRNN model includes the following three aspects: (a) The fruit fly optimization algorithm achieves the goal of finding the global optimal solution of complex functions in space by simulating the competition and cooperation behavior of fruit fly individuals. The algorithm has the advantages of simple calculation process and fast convergence speed. (b) Generalized regression neural network (GRNN) has the advantages of strong nonlinear mapping ability, single setting parameters, high fault tolerance, and robustness and has high prediction accuracy and stability. (c) The GRNN algorithm is easy to fall into the shortcoming of local optimum. The CFOA algorithm can find the global optimal solution for complex functions in space, and the CFOA algorithm is combined with the GRNN prediction model to make up for the shortcomings of the GRNN algorithm that is easy to fall into local optimality, quickly find the global optimal solution, and improve the prediction efficiency. And accuracy can be greatly improved. The prediction results can provide reference for prediction of floor water inrush and safe production of working faces.

2. Influencing Factors of Floor Water Inrush in Coal Mines

2.1. Aquifer Pressure. Head pressure of confined aquifers below coal floors is the precondition and power for floor

water inrush. To cause floor water inrush, the head pressure of underlying aquifers should be large enough. Under the same conditions of the aquifuge for coal floors, the confined water pressure below coal floors is directly proportional to the probability of occurrence of water inrush. Particularly, when the aquifuge is affected by mining activities or encounters a fault, the water pressure exerts significant influences on water inrush. Therefore, aquifer pressure is an important basis from which to study floor water inrush.

2.2. Aquifuge Thickness. An aquifuge for coal floors is an intact stratum between a coal floor and the top of an aquifer. The aquifuge exerts influences different from other factors and plays a critical role in preventing groundwater of a confined aquifer from entering the mining space of a mine. It is the only inhibiting factor for floor water inrush and forms a safety barrier for mining above confined aquifers.

Aquifuges can obstruct floor water inrush, and the capability depends on aquifuge thickness, mechanical strength of rock, and integrity of aquifuges. When keeping other conditions unchanged, the thicker and the stronger the aquifuge, the lower the probability of water inrush, and *vice versa* [15]. According to statistical analysis of 343 water-inrush records in typical mining areas in China, the relationship between the aquifuge thickness and the number of water inrush is revealed (Table 1).

2.3. Dip Angle of Coal Seams. According to dip angles, coal seams can be classified into nearly horizontal, gently inclined, inclined, deeply inclined, and steeply inclined, separately corresponding to dip angles of less than 8°, between 8~25°, 25~45°, and 35~65°, and greater than 45°. Previous research has shown that when the dip angle of faults is small, shear failure is likely to occur during coal mining, which induces fractures in aquifers and finally water-inrush accidents. Numerous engineering cases have proven that deeply inclined coal seams are more likely to encounter water-inrush accidents.

2.4. Fault Throw. Damage of faults to coal and rock mass is mainly manifest as increased fractures and pores in, and greatly decreased strength of, coal and rock mass nearby a fault. Different fault throws may produce different contact relationships between coal seams and aquifers in two plates of a fault. Analysis shows that the larger the fault throw and the deeper the cut, the greater the influences of faults and the greater the probability of floor water inrush.

Mining conditions such as mining height and mining methods also affect the initial stress state of the coal and rock mass and the damage depth of coal floors and further influence floor water inrush. Six factors including water pressure (MPa), mining height (m), aquifuge thickness (m), fault throw (m), dip angle of coal seams (°), and distance from a fault to a working face (m) are taken as main influencing factors of floor water inrush. The original data selected are listed in Table 2. The sample data is obtained from the statistics of some mines in my country, mainly including the water-inrush data from the working face and floor of the typical large-water mining areas, such as Hebei Fengfeng, Jinglong, Hebi Hebi, and Shandong Zibo, and the measured data of normal mining.

Table 1: Relationship between aquifuge thickness and number of water inrush in typical mining areas.

Aquifuge thickness (m)	Number of water-inrush events	Proportion (%)
>40	23	7
32-40	34	10
25-32	96	28
20-25	77	22
<20	113	33

3. Principles Underpinning Various Algorithms

3.1. CFOA. Fruit flies can accurately locate distant food sources because of their special sense organs. The fruit fly optimization algorithm (FOA) is an algorithm deduced for searching for the optimal results based on foraging behaviors of fruit flies. FOA simulates the optimization process of fruit flies according to their foraging behavior and then finds the optimal solution. It is characterized by advantages including understandable logic, no need to adjust data and parameters, and rapid convergence [36–38]. When searching in a complex environment, FOA is likely to be trapped in local extremums and leads to a large deviation between the results and reality. FOA has been applied in neural network training [39], financial distress model solving [40], power load forecasting [41], multidimensional knapsack problem [42], web auction logistics service [43], and so on [44–46].

Chaos theory is universal in its applicability to such problems, and its methods can avoid being trapped in local extrema. Therefore, the CFOA is used to compensate for the drawback of the FOA. The steps are briefly described as follows:

Step 1. The initial location (InitX, InitY) of a fruit fly is randomly determined.

Step 2. Random directions and distances are assigned to fruit flies to search for food.

$$\begin{aligned} X_i &= \text{InitX} + \text{Random value}, \\ Y_i &= \text{Inity} + \text{Random}. \end{aligned} \tag{1}$$

Step 3. The distance (Dist) of a fruit fly to the origin is estimated, and then, the judgment value of smell concentration (S) is calculated, which is the reciprocal of the distance.

$$\begin{aligned} \text{Dist} &= \sqrt{x^2 + y^2}, \\ S &= \frac{1}{\text{Dist}}. \end{aligned} \tag{2}$$

Step 4. The judgment value of smell concentration (S) is substituted into the judgment function of smell

Table 2: Original data pertaining to influencing factors.

Serial no.	Water pressure (MPa)	Mining height (m)	Aquifuge thickness (m)	Fault throw (m)	Dip angle of coal seams (°)	Distance from a fault to a working face (m)	Water-inrush level
1	1.82	0.8	26.39	4	12	16	I
2	1.65	1.6	25.85	50	17	90	II
3	1	0.9	22.33	2	13	16	II
4	2.88	1	17.68	1.3	20	0	II
5	2.01	8	28	0.6	18	10	III
6	1.91	8	43	1.5	11	2	III
7	1.33	0.85	36.28	0.8	7	62	I
8	0.95	1.45	26.89	1	6	55	I
9	0.92	1.4	33.61	0.5	8	0	I
10	0.34	0.9	32.65	22	6	6	I
11	1.06	2	27.79	0.46	7	21	I
12	0.83	2.85	26.56	0.7	12	6	I
13	2	2.81	30	1.5	18	12	IV
14	1.8	1.9	23	0	15	17	IV
15	1.7	2.8	10	5	17	10	II
16	0.6	1.1	17	2	19	6	I
17	2.1	1.6	59.5	3.5	10	39	I
18	2.8	2.75	69.17	11.7	12	36	I
19	2.8	2.55	66.11	16	12	29	I
20	1.3	1.7	30	4.9	5	21	II
21	1.08	0.9	16.5	3.2	7	7	II
22	1.01	0.9	16.5	3.2	14	75	II
23	2.01	8	28	0.6	18	10	II
24	1.91	8	43	1.5	11	2	I
25	2.55	8	50	4	13	10	I
26	2.35	2	50	100	16	153	I
27	0.69	3.85	42	32	12	19	III
28	1.68	5	35.3	7	16.7	20	II
29	1.67	5	35.4	7	16.4	12.4	II
30	1.82	5	34.5	7	16.5	0	II
31	1.75	5	34.6	7	13	6	II
32	1.7	5	34.8	7	12.5	12	IV
33	1.77	5	35	8	12	95	I
34	1.67	5	35.3	8	10	96	I
35	1.62	5	36	8	9	103	I
36	1.74	5	34.1	7	20	27	II
37	1.75	5	33.7	7	13	24	II
38	1.82	5	33.6	7	13.4	32	II
39	1.87	5	33.6	7	11	44	I
40	1.84	5	33.8	7	11	55	I
41	1.79	5	34	8	11.5	53	III
42	1.77	5	34.2	8	10.7	45	III
43	1.75	5	34.5	8	10.5	44.8	II
44	1.7	5	34.8	8	13	51	II
45	1.82	5	33.1	7	12	77	I
46	1.87	5	32.6	7	17	74	II
47	1.94	5	32.6	7	15.5	81	II
48	1.97	5	32.8	7	9.5	93	III

Table 2: Continued.

Serial no.	Water pressure (MPa)	Mining height (m)	Aquifuge thickness (m)	Fault throw (m)	Dip angle of coal seams (°)	Distance from a fault to a working face (m)	Water-inrush level
49	1.1	1.6	20	15	11	16	I
50	4.06	2.75	65.86	10	10	11	II
51	3.11	2.61	44.3	3.5	11	12	II
52	2.7	2.55	66.97	16	12	31	II
53	2.3	1.5	46.91	1	11	24	III
54	1.91	1.5	43.11	1.1	8	130	III
55	1.45	1.5	38.9	3	13.5	27	IV
56	1.5	1.5	38.9	1.2	13.5	7	IV
57	1.78	1.5	38.9	11	14	36	II
58	0.74	7.5	65	79	11	63	I
59	1.37	8	50	15	14	15	I
60	1.45	8	46	2.5	15	9	II

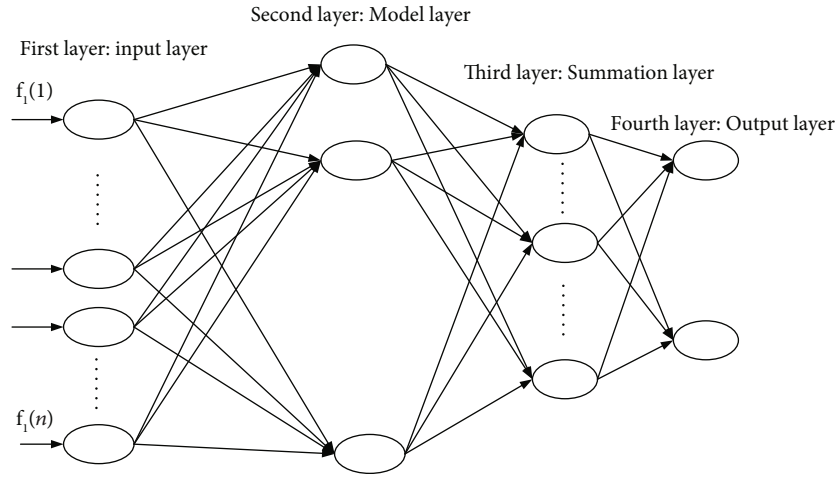

Figure 1: GRNN structure.

concentration to calculate smell concentration (smell) at the individual locations of each fruit fly.

Step 5. The fruit fly with the highest smell concentration in the population is found.

Step 6. The location of the fruit fly with the optimal smell concentration is retained, to which the fruit fly population flies.

Step 7. Iterative optimization is conducted, and Steps 2~5 are repeated. Whether the smell concentration is better than the previous iteration or not is judged. If yes, Step 6 is performed; otherwise, the prediction results are output.

Chaos Fruit Fly Optimization Algorithm (CFOA) is the optimal position of each generation obtained in the iterative optimization process of the fruit fly optimization algorithm, adding chaotic disturbance and performing secondary optimization, which can make the population jump out of the local optimal solution, implementing global search. Other variants of FOA often fall into local extrema when searching for complex environments, which affects the computational accuracy and efficiency.

3.2. GRNN. GRNN is based on the nonparametric kernel regression and allows nonparametric estimation taking sample data as the verification condition of posterior probability, so it has favorable learning ability. The most prominent advantage of GRNN is the setting of network parameters which is so convenient that its network performance can be adjusted only by setting the smoothing factor in the kernel function. The first layer of the GRNN is an input layer, on which the number of neurons is same as the dimensions of the input vectors of learning samples and each neuron is a simple distributed network unit. These neurons directly transfer the input variables into the hidden layer. GRNN uses sample data as the verification condition for posterior probability and nonparametric estimation. Finally, to obtain the regression of dependent variables relative to independent variables, the correlation density function between

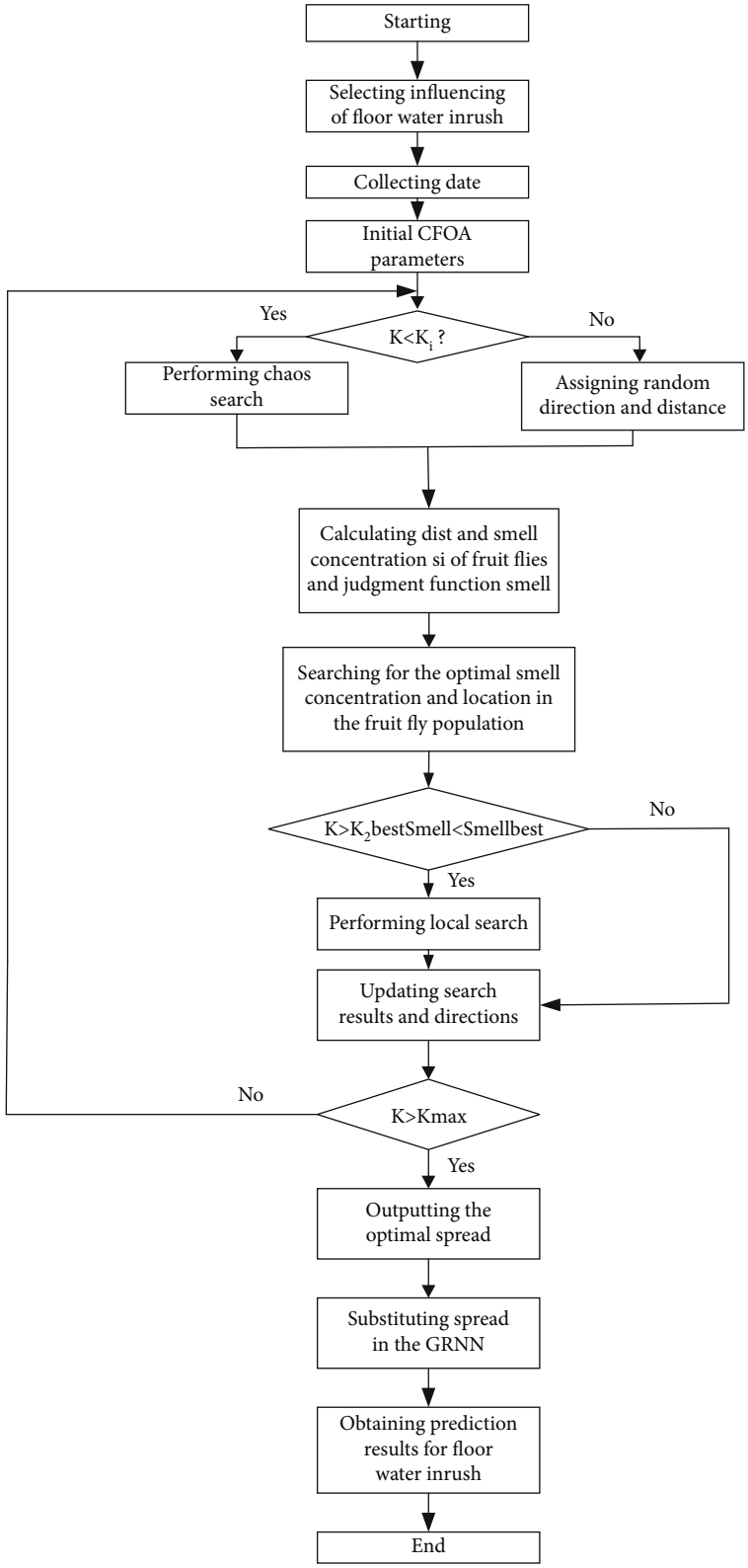

Figure 2: Flowchart of the CFOA–GRNN prediction model.

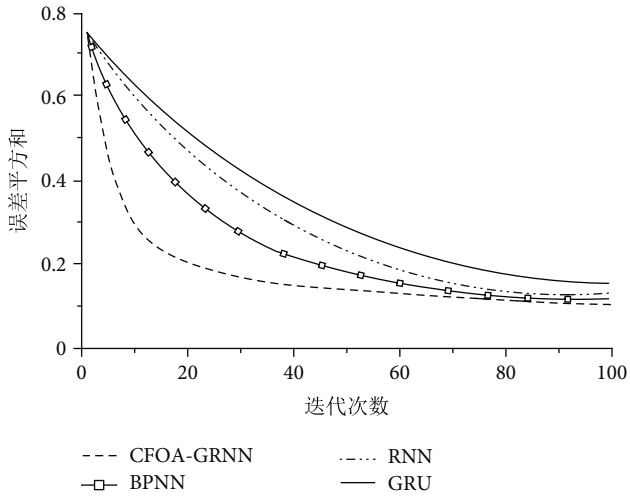

Figure 3: Network training error curve.

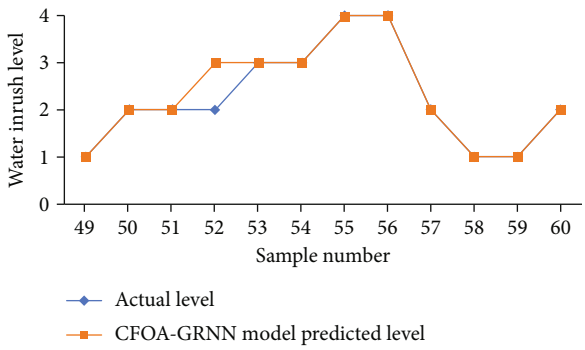

Figure 4: Prediction results of the CFOA-GRNN model.

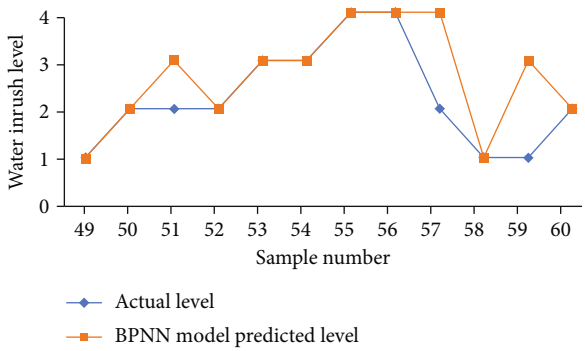

Figure 5: Prediction results of the BPNN model.

dependent variables and independent variables in the GRNN is calculated using the training samples. The calculation formula is shown as follows:

$$\bar{Y} = E(Y/X) = \frac{\int_{-\infty}^{+\infty} yf(X,Y)dY}{\int_{-\infty}^{+\infty} f(X,Y)dY}. \tag{3}$$

For an unknown probability density function $f(X, Y)$,

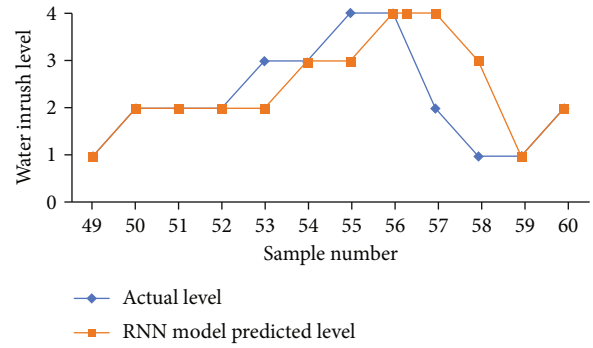

Figure 6: Prediction results of the RNN model.

the following formula is obtained through nonparametric estimation:

$$\bar{f}(X,Y) = \frac{1}{(2\pi)^{(p+1/2)}\delta^{(p+1)}n} \times \sum_{i=1}^{n} \exp\left[-\frac{(X-X_i)^T(X-X_i)}{2\delta^2}\right] \exp\left[-\frac{Y-Y_i}{2\delta^2}\right], \tag{4}$$

where X_i and Y_i separately refer to the observed values of random variables X and Y, δ is a smoothing factor, and n and p separately denote the sample size and dimension of x. The following can be attained according to Formulae (3) and (4):

$$\bar{Y} = \frac{\sum_{i=1}^{n} Y_i \exp\left[-\left((X-X_i)^T(X-X_i)\right)/2\delta^2\right] \int_{-\infty}^{+\infty} y \exp\left[-(y-Y_i)^2/2\delta^2\right]dy}{\sum_{i=1}^{n} Y_i \exp\left[-(X-X_i)^T(X-X_i)/2\delta^2\right] \int_{-\infty}^{+\infty} \exp\left[-(y-Y_i)^2/2\delta^2\right]dy}. \tag{5}$$

This can be simplified to

$$\bar{Y} = \frac{\sum_{i=1}^{n} Y_i \exp\left[-(X-X_i)^T(X-X_i)/2\delta^2\right]}{\sum_{i=1}^{n} \exp\left[-(X-X_i)^T(X-X_i)/2\delta^2\right]}. \tag{6}$$

Formula (6) is the expression for the final output of the GRNN. Based on the calculation formula, the output error of the GRNN is mainly dependent on its smoothing factor δ. When the smoothing factor is very large, $\bar{Y}$ tends to the mean of dependent variables of all samples; on the contrary, if the smoothing factor tends to 0, $\bar{Y}$ is approximated to the training samples. Dependent variables of all samples can be considered only when δ is set to a moderate value, thus obtaining favorable results. Therefore, satisfactory results can be obtained by simply adjusting the smoothing factor of the prediction model. The structure of the GRNN is illustrated in Figure 1.

4. Establishment and Analysis of the Model for Floor Water Inrush Based on CFOA–GRNN

4.1. Model Establishment. CFOA features excellent search capability, which is used to optimize the GRNN model. The basic idea of optimizing GRNN with CFOA is to

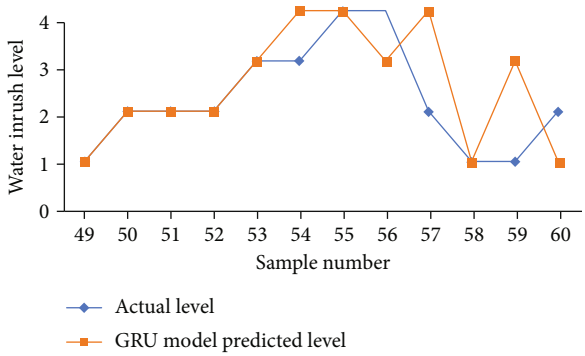

Figure 7: Prediction results of the GRU model.

convert the distance between a fruit fly and the origin into the smoothing factor (through use of the neural network toolbox in MATLAB™); through training of the GRNN model, the output samples are attained; the prediction error of GRNN is used as the judgment function of smell concentration to find the location of the individual with the lowest error corresponding to all smoothing factors; the above operation is repeated until the condition of convergence is met or the maximum number of iterations is reached. The specific steps are shown as follows:

(1) Influencing factors are selected and data collected

(2) The initial position (Init$X$,Init$y$) of a fruit fly is set at random, which searches within the range (X min, Xmax), (Y min, Ymax). After adding chaotic disturbance C, searched locations of the fruit fly can be obtained on the X and Y-axes

$$\begin{aligned} X_{\text{axis}} &= \text{Init}X(i) + C(\bullet) \\ Y_{\text{axis}} &= \text{Init}Y(i) + C(\bullet) \end{aligned} \tag{7}$$

(3) The distance $D(i)$ between the fruit fly and the origin is calculated according to coordinates of the fruit fly

$$D(i) = \sqrt{x^2 + y^2} \tag{8}$$

(4) The calculation function of smell concentration is determined using the distance function $D(i)$, and the optimal fitness function is searched. The fitness function is updated, and the variable values are optimized. Then, the local optimal location of the fruit fly is sought in accordance with the chaotic sequences

Table 3: Comparison of the evaluation results of each model.

Parameters	RNN	BPNN	GRU	CFOA-GRNN
OA/%	66.7	75	58.3	91.7
LA(1)/%	66.7	66.7	66.7	100
LA(2)/%	80	60	60	80
LA(3)/%	50	100	50	100
LA(4)/%	50	100	50	100
Tm/s	5.1	4.66	4.8	3.78

$$\begin{aligned} X(i) &= X\text{axis}c + (2\ \text{rand}\ () - 1)C(\bullet) \\ Y(i) &= Y\text{axis}c + (2\ \text{rand}\ () - 1)C(\bullet) \end{aligned} \tag{9}$$

(5) After finishing the iterative loop, the location of the fruit fly with the largest coverage is recorded, and the maximum smell concentration is retained

$$\begin{cases} X\text{axis}c = X(\text{bestindex}) \\ Y\text{axis}c = Y(\text{bestindex}) \\ \text{Smellbest} = \text{bestSmell} \end{cases} \tag{10}$$

(6) Search of the CFOA is stopped when the number of iterations K is bigger than K max; otherwise, the operation returns to Step 2 to collect the spread of GNRR

(7) The GRNN model is established, and the optimized spread is used to train the network

The specific prediction steps are shown in Figure 2.

4.2. Model Analysis. The first 48 sample data are selected as the training data for the CFOA–GRNN prediction model for floor water inrush and late 12 data as the samples for prediction. The fruit flies are initially at [0,1], and the fruit fly population is 25. The number of maximum iterations and the disturbance factor Dist are set to 150 and 0.5313, respectively. After 98 iterations, the root-mean-square error (RMSE) is 0.0636, and the optimal spread of the CFOA is 0.0076. The obtained optimal spread is substituted in the GRNN to predict floor water-inrush risk. In order to verify the superiority of the performance of the CFOA-GRNN model, the training and prediction effects of the FOA-GRNN model, BPNN model, RNN model, and GRU model are compared with it. Figure 3 shows the training error curves of each model. As can be seen from Figure 4, compared with the other three models, the CFOA-GRNN prediction model has a faster optimization and convergence speed, and the prediction error is relatively stable.

Water-inrush level of the 12 groups of data that occurred last in the sample set, that is, the 49th-60th group of sample data, was selected for testing. Establish CFOA-GRNN,

BPNN, RNN, and GRU network prediction models, and compare the prediction results with the real situation, see Figures 4–7 for details.

For the analysis of the evaluation results, the following evaluation indicators can be used to evaluate the feasibility and pros and cons of the model.

(1)Overall accuracy (OA) refers to the proportion of the number of correctly classified samples to the total number of samples, which reflects the accuracy of the model's prediction of all levels. The expression is as follows:

$$\mathrm{OA} = \frac{N_c}{N_t} \times 100\% \tag{11}$$

In the formula, N_t is the total number of test samples, and N_t is the number of samples whose predicted level is equal to the original level of the Nc model.

(2)Local accuracy (LA) refers to the ratio of the number of correctly classified samples of the ith level to the total number of samples of the $i$level, reflecting the accuracy of the model's prediction of a certain level, and its expression is as follows:

$$\mathrm{LA}(i) = \frac{N(i)_c}{N(i)_t} \times 100\%, \ (i = 1, 2, 3, 4) \tag{12}$$

In the formula, $\mathrm{LA}(i)$ is the accuracy of water-inrush level i, $N(i)_t$ is the number of test samples with water-inrush level i, and $N(i)_c$ is the number of samples at level i equal to the original level.

(3)Operation time T: it reflects the operation speed of the model

The prediction results of the model are evaluated using the above evaluation indicators, and the evaluation results are shown in Table 3. In terms of overall accuracy, the overall accuracy of the CFOA-GRNN model is 16.7% higher than that of the BPNN model, 25% higher than that of the RNN model, and 33.4% higher than that of the GRU model. From the perspective of local accuracy, the introduction of CFOA can effectively improve the local accuracy of the neural network model for the prediction of water inrush at each level and greatly improve the prediction accuracy of the water inrush from the floor. In terms of operation time Tm, the operation time of the CFOA-GRNN model is 18.9% less than that of the BPNN model, 25.9% less than that of RNN, and 21.3% less than that of GRU. Therefore, in summary, the introduction of CFOA can greatly improve the accuracy of the GRNN neural network prediction model for water inrush from the bottom of the model and also significantly reduce the computing time.

Compared with the prediction results of the other three algorithms, it can be seen that the overall accuracy of the other three prediction models is not high. The overall accuracy of the BPNN neural network prediction model, the RNN neural network prediction model, and the GRU (gated recurrent unit) neural network prediction model is 75%, 66.7%, and 58.3%, while the overall accuracy of the CFOA-GRNN neural network prediction model is 91.7%. From the perspective of $\mathrm{LA}(i)$, the local accuracy of the CFOA-GRNN neural network prediction model introduced with the chaotic fruit fly optimization algorithm is also significantly improved compared with the other three neural network prediction models. The superiority of the proposed prediction model is confirmed from the three aspects of overall accuracy, local accuracy, and computation time. The prediction result of CFOA-GRNN model on whether water inrush occurs in actual engineering is very close to the actual situation, and its accuracy is significantly higher than that of the other three models. This result shows that the CFOA-GRNN model is reliable in predicting whether there is a risk of water inrush from the floor in actual engineering.

5. Conclusion

In order to solve the floor water-inrush issue, CFOA-GRNN model is established to predict floor water inrush based on the theory of nonlinear regression by combining relevant water-inrush data of numerous working faces and derived the following conclusions:

(1) The prediction effect of GRNN is affected by the smoothing factor, so the CFOA is used to optimize the smoothing factor, which reduces influences of human factors on the parameter determination in the GRNN prediction model and improves the prediction accuracy and applicability of the model

(2) By comprehensively analyzing causes of floor water inrush, six main factors are selected to construct the CFOA–GRNN prediction model for floor water inrush

(3) The accuracy of the CFOA–GRNN prediction model is 91.7%, the established prediction model has a high accuracy, and the prediction results are in agreement with reality, so it can be used to predict floor water inrush in coal mines in China to guide safe production

(4) In the established CFOA-GRNN model, it is found that the fruit fly search function has a great influence on the convergence of the prediction results. In future research, the optimization of the fruit fly search function will be explored in depth to reduce the prediction error caused by the change of the search function

Data Availability

The original contributions presented in the study are included in the article, and further inquiries can be directed to the corresponding author.

Conflicts of Interest

The authors declare that they have no conflicts of interest.

Acknowledgments

The authors acknowledge the State Key Laboratory of Coal Resources in Western China (SKLCRKF1913), the Basic Scientific Research Projects of Universities in Liaoning Province (LJKZ0343), and State Key Laboratory of Coal Mining and Clean Utilization (2021-CMCU-KF016).

References

[1] B. Zhao, G. Wen, J. Nian et al., "Numerical simulation study on the multi-physical field response to underground coal and gas outburst under high geo-stress conditions," *Minerals*, vol. 12, no. 2, p. 151, 2022.

[2] Z. Wen, E. Xing, S. Shi, and Y. Jiang, "Overlying strata structural modeling and support applicability analysis for large mining-height stopes," *Journal of Loss Prevention in the Process Industries*, vol. 57, pp. 94–100, 2019.

[3] X. Li, Q. Guo, and S. Liu, "Influence of steel fiber on durability performance of concrete under freeze- thaw cycles," *Advances in Materials Science and Engineering*, vol. 2021, Article ID 5460844, 12 pages, 2021.

[4] X. Li, Z. Cao, and Y. Xu, "Characteristics and trends of coal mine safety development," *Energy Sources Part a-Recovery Utilization and Environmental Effects*, pp. 1–19, 2020.

[5] C. Fan, H. Wen, S. Li, G. Bai, and L. Zhou, "Coal seam gas extraction by integrated drillings and punchings from the floor roadway considering hydraulic-mechanical coupling effect," *Geofluids*, vol. 2022, Article ID 5198227, 10 pages, 2022.

[6] B. Zhao, G. Wen, Q. Ma, H. Sun, F. Yan, and J. Nian, "Distribution characteristics of pulverized coal and stress–gas pressure–temperature response laws in coal and gas outburst under deep mining conditions," *Energy Science & Engineering*, pp. 1–19, 2022.

[7] K. Xiao, Z. Zhang, R. Zhang et al., "Anisotropy of the effective porosity and stress sensitivity of coal permeability considering natural fractures," *Energy Reports*, vol. 7, pp. 3898–3910, 2021.

[8] Z. Wen, S. Jing, Y. Jiang et al., "Study of the fracture law of overlying strata under water based on the flow- stress-damage model," *Geofluids*, vol. 2019, 12 pages, 2019.

[9] X. Wang, Z. Wen, Y. Jiang, and H. Huang, "Experimental study on mechanical and acoustic emission characteristics of rock-like material under non-uniformly distributed loads," *Rock Mechanics and Rock Engineering*, vol. 51, no. 3, pp. 729–745, 2018.

[10] S. Liu, X. Li, D. Wang, and D. Zhang, "Investigations on the mechanism of the microstructural evolution of different coal ranks under liquid nitrogen cold soaking," *Energy Sources Part a-Recovery Utilization and Environmental Effects*, pp. 1–17, 2020.

[11] X.-l. Li, S.-j. Chen, S.-m. Liu, and Z.-h. Li, "AE waveform characteristics of rock mass under uniaxial loading based on Hilbert-Huang transform," *Journal of Central South University*, vol. 28, no. 6, pp. 1843–1856, 2021.

[12] X. Li, S. Chen, Q. Zhang, X. Gao, and F. Feng, "Research on theory, simulation and measurement of stress behavior under regenerated roof condition," *Geomechanics and Engineering*, vol. 26, no. 1, pp. 49–61, 2021.

[13] Z. Jia, H. Xie, R. Zhang et al., "Acoustic emission characteristics and damage evolution of coal at different depths under triaxial compression," *Rock Mechanics and Rock Engineering*, vol. 53, no. 5, pp. 2063–2076, 2020.

[14] C. Fan, L. Yang, G. Wang, Q. Huang, X. Fu, and H. Wen, "Investigation on coal skeleton deformation in CO_2 injection enhanced CH4 drainage from underground coal seam," *Frontiers in Earth Science*, vol. 9, pp. 1–11, 2021.

[15] T. Ai, S. Wu, R. Zhang et al., "Changes in the structure and mechanical properties of a typical coal induced by water immersion," *International Journal of Rock Mechanics and Mining Sciences*, vol. 138, article 104597, 2021.

[16] Z. Zhu, Y. Wu, and J. Han, "A prediction method of coal burst based on analytic hierarchy process and fuzzy comprehensive evaluation," *Frontiers in Earth Science*, vol. 9, pp. 1–12, 2022.

[17] Y. Hu, W. Li, Q. Wang, S. Liu, and Z. Wang, "Evolution of floor water inrush from a structural fractured zone with confined water," *Mine Water and the Environment*, vol. 38, no. 2, pp. 252–260, 2019.

[18] Z. Ji, H. Tian, Z. Yang, T. Liu, and S. Bandara, "Mechanism of water inrush from coal seam floor based on coupling mechanism of seepage and stress," *Journal of Intelligent & Fuzzy Systems*, vol. 34, no. 2, pp. 965–974, 2018.

[19] S. Zhang, W. Guo, and Y. Li, "Experimental simulation of water-inrush disaster from the floor of mine and its mechanism investigation," *Arabian Journal of Geosciences*, vol. 10, no. 22, p. 503, 2017.

[20] S. Zhang, W. Guo, Y. Li, W. Sun, and D. Yin, "Experimental simulation of fault water inrush channel evolution in a coal mine floor," *Mine Water and the Environment*, vol. 36, no. 3, pp. 443–451, 2017.

[21] S. C. Li, J. Wu, Z. H. Xu, and W. M. Yang, "Mechanics criterion of water inrush from the coal floor under influence of fault and its engineering application," *International Journal of Geomechanics*, vol. 19, no. 5, pp. 1–9, 2019.

[22] T. Li and C. Wang, "Numerical simulation study on formation and evolution process of water-inrush channel in floor under high water pressure," *Geotechnical and Geological Engineering*, vol. 37, no. 4, pp. 3007–3012, 2019.

[23] K. Ma, X. Y. Sun, C. A. Tang, F. Z. Yuan, S. J. Wang, and T. Chen, "Floor water inrush analysis based on mechanical failure characters and microseismic monitoring," *Tunnelling and Underground Space Technology*, vol. 108, article 103698, 14 pages, 2021.

[24] A. J. Shao, J. P. Peng, Q. X. Meng, and Y. Huang, "Catastrophic model of water inrush from coal mine floor," *Applied Mechanics and Materials*, vol. 316-317, pp. 1106–1111, 2013.

[25] Z. Feng-da, S. H. Bao-hong, and K. A. Yong-hua, "Water inrush failure mechanism of mining floor under unloading effect," *Rock and Soil Mechanics*, vol. 37, no. 2, pp. 431–438, 2016.

[26] Y. Zhang and L. Yang, "A novel dynamic predictive method of water inrush from coal floor based on gated recurrent unit model," *Natural Hazards*, vol. 105, no. 2, pp. 2027–2043, 2021.

[27] G.-d. Zhang, Y.-g. Xue, C.-h. Bai, M.-x. Su, K. Zhang, and Y.-f. Tao, "Risk assessment of floor water inrush in coal mines based on MFIM-TOPSIS variable weight model," *Journal of Central South University*, vol. 28, no. 8, pp. 2360–2374, 2021.

[28] J. Zhang, Q. Wu, W. Mu, Y. du, and K. Tu, "Integrating the hierarchy-variable-weight model with collaboration-competition theory for assessing coal-floor water-inrush risk," *Environmental Earth Sciences*, vol. 78, no. 6, pp. 50–55, 2019.

[29] D. Zhao, Q. Wu, F. Cui et al., "Using random forest for the risk assessment of coal-floor water inrush in Panjiayao Coal Mine, northern China," *Hydrogeology Journal*, vol. 26, no. 7, pp. 2327–2340, 2018.

[30] D. Dong, Z. Chen, G. Lin, X. Li, R. Zhang, and Y. Ji, "Combining the fisher feature extraction and support vector machine methods to identify the water inrush source: a case study of the Wuhai mining area," *Mine Water and the Environment*, vol. 38, no. 4, pp. 855–862, 2019.

[31] Y. Wang, M. R. Zhou, P. C. Yan, C. Y. He, and D. Liu, "Identification of coalmine water inrush source with PCA-BP model based on laser-induced fluorescence technology," *Spectroscopy and Spectral Analysis*, vol. 37, no. 3, pp. 978–983, 2017.

[32] B. Wu, L. Wang, S. Wang, and Y. R. Zeng, "Forecasting the U.S. oil markets based on social media information during the COVID-19 pandemic," *Energy*, vol. 226, pp. 120403–120420, 2021.

[33] G. E. Lee and A. Zaknich, "A mixed-integer programming approach to GRNN parameter estimation," *Information Sciences*, vol. 320, pp. 1–11, 2015.

[34] J. Zhao, H. Guan, C. Lu, and Y. Zheng, "Evaluation of teachers' educational technology ability based on fuzzy clustering generalized regression neural network," *Computational Intelligence and Neuroscience*, vol. 2021, Article ID 1867723, 10 pages, 2021.

[35] L. Wang, T. J. Lee, J. Bavendiek, and L. Eckstein, "A data-driven approach towards the full anthropometric measurements prediction via generalized regression neural networks," *Applied Soft Computing*, vol. 109, article 107551, 2021.

[36] R.-Y. Wang, P. Hu, C. C. Hu, and J. S. Pan, "A novel fruit fly optimization algorithm with quasi-affine transformation evolutionary for numerical optimization and application," *International Journal of Distributed Sensor Networks*, vol. 18, no. 2, 2022.

[37] L. Wang, Y. Xiong, S. Li, and Y. R. Zeng, "New fruit fly optimization algorithm with joint search strategies for function optimization problems," *Knowledge-Based Systems*, vol. 176, pp. 77–96, 2019.

[38] S.-X. Lv, Y.-R. Zeng, and L. Wang, "An effective fruit fly optimization algorithm with hybrid information exchange and its applications," *International Journal of Machine Learning and Cybernetics*, vol. 9, no. 10, pp. 1623–1648, 2018.

[39] P.-W. Chen, W. Y. Lin, T. H. Huang, and W. T. Pan, "Using fruit fly optimization algorithm optimized Grey model neural network to perform satisfaction analysis for E-business service," *Applied Mathematics & Information Sciences*, vol. 7, no. 2L, pp. 459–465, 2013.

[40] W.-T. Pan, "A new fruit fly optimization algorithm: taking the financial distress model as an example," *Knowledge-Based Systems*, vol. 26, pp. 69–74, 2012.

[41] H. Li, S. Guo, H. Zhao, C. Su, and B. Wang, "Annual electric load forecasting by a least squares support vector machine with a fruit fly optimization algorithm," *Energies*, vol. 5, no. 11, pp. 4430–4445, 2012.

[42] L. Wang, X.-l. Zheng, and S.-y. Wang, "A novel binary fruit fly optimization algorithm for solving the multidimensional knapsack problem," *Knowledge-Based Systems*, vol. 48, pp. 17–23, 2013.

[43] S.-M. Lin, "Analysis of service satisfaction in web auction logistics service using a combination of fruit fly optimization algorithm and general regression neural network," *Neural Computing & Applications*, vol. 22, no. 3-4, pp. 783–791, 2013.

[44] L. Wu, Q. Liu, X. Tian, J. Zhang, and W. Xiao, "A new improved fruit fly optimization algorithm IAFOA and its application to solve engineering optimization problems," *Knowledge-Based Systems*, vol. 144, pp. 153–173, 2018.

[45] S. Kanarachos, J. Griffin, and M. E. Fitzpatrick, "Efficient truss optimization using the contrast-based fruit fly optimization algorithm," *Computers & Structures*, vol. 182, pp. 137–148, 2017.

[46] Z. He, H. Qi, Y. Yao, and L. Ruan, "Inverse estimation of the particle size distribution using the fruit fly optimization algorithm," *Applied Thermal Engineering*, vol. 88, pp. 306–314, 2015.